Non-resonant and resonant X-ray emission at high pressure using a von Hámos setup: the case of FeO

Journal of Physics: Conference Series **2380** (2022) 012128 doi:10.1088/1742-6596/2380/1/012128

Non-resonant and resonant X-ray emission at high pressure using a von Hámos setup: the case of FeO

Christian Albers,[1,*] Nicola Thiering,[1] Robin Sakrowski,[1] Hlynur Gretarsson,[2,3] Johannes Kaa,[1,4] Martin Sundermann,[2,3] Metin Tolan,[1,5] Max Wilke,[6] Christian Sternemann[1,*]

[1]Fakultät Physik/DELTA, Technische Universität Dortmund, 44227 Dortmund, Germany
[2]Max Planck Institute for Chemical Physics of Solids, 01187 Dresden, Germany
[3]PETRA III, Deutsches Elektronen-Synchrotron (DESY), 22607 Hamburg, Germany.
[4]European X-Ray Free-Electron Laser Facility GmbH, 22869 Schenefeld, Germany
[5]Universität Göttingen, 37073 Göttingen, Germany
[6]Institut für Geowissenschaften, Universität Potsdam, 14476 Potsdam, Germany

E-mail: *christian2.albers@tu-dortmund.de and christian.sternemann@tu-dortmund.de

Abstract. We present a setup exploiting a von Hámos spectrometer in order to study (resonant) X-ray emission of matter exposed to high pressure. The capabilities of this setup are demonstrated for the case of FeO at pressures between 13 GPa and 75 GPa. The setup provides high-quality K$\beta_{1,3}$ X-ray emission spectra at high pressures for iron spin state analysis within minutes and iron valence-to-core spectra in less than one hour. Resonant X-ray emission maps can be obtained on a timescale of one hour with 1.0 eV and in approximately 3 hours with 0.2 eV incident energy resolution. Both Kα and Kβ emission can be utilized to gain L-edge and M-edge-like information, respectively, with the option of measuring both simultaneously. The spin state results on FeO between 13 GPa and 75 GPa are in accordance with recent literature. The structural distortion is reflected in both, valence-to-core spectra and resonant X-ray emission maps, which showcase the great potential of the presented setup. The achieved data acquisition times are promising to couple pressure with temperature by laser heating.

1. Introduction

The knowledge of the electronic structure of iron-bearing compounds at pressure and temperature is important for understanding the Earth's geochemical processes owing to iron's abundance in the Earth's mantle. Iron appears in two different oxidation states as ferrous and ferric iron, i.e., Fe^{2+} and Fe^{3+}. Due to its electronic complexity and appearance in various structurally diverse compositions, it can affect physical and chemical properties of the deep Earth. Iron's pressure-induced spin transition for example influences the sound velocity and compressibility of the materials and can furthermore affect the element partitioning in the Earth's mineral assemblages [1, 2, 3, 4].

An important compound in this context is the iron-oxide wüstite (FeO). It is known that FeO undergoes a structural transition from cubic ($Fm\bar{3}m$) to rhombohedral (R$\bar{3}$m) crystal symmetry at 16 GPa and at higher pressures of about 100 GPa to the B8 phase with a NiAs-type structure [5, 6, 7, 8]. Its electronic structure has been investigated mainly in mixed (Mg,Fe)O crystal systems with a variety of experimental approaches like Mössbauer spectroscopy

[9, 10, 11, 12, 13, 14, 15], (resonant) X-ray emission spectroscopy ((R)XES) [16, 17, 18, 19], and optical absorption spectroscopy [20, 21, 22]. However, some studies particularly investigated the pure FeO system. Badro et al. [23] found no complete spin transition from high-spin (HS) to low-spin (LS) state up to a pressure of 143 GPa via K$\beta_{1,3}$ XES, even though the K$\beta_{1,3}$ line shape changes significantly, whereas Ozawa et al. [24] report a nearly full spin transition occurring between 103 GPa and 119 GPa. Hamada et al. [25] and Pasternak et al. [26] obtained by Mössbauer spectroscopy a slow pressure-induced spin decrease starting at around 90 GPa. In the following, we present iron K$\beta_{1,3}$ and valence-to-core (vtc) XES spectra of pure FeO measured up to a pressure of 75 GPa. At 13 GPa in the cubic and 75 GPa in the rhombohedral phase, we additionally acquired 1s2p RXES maps. The results are discussed in terms of changes in electronic structure with emphasis on spin state changes.

2. Materials and Methods

Synthetic $Fe_{0.94}O$ (FeO from here on) was loaded into a BX90 Diamond Anvil Cell (DAC) with a radial opening (BX90-RO). The DAC was equipped with a standard diamond (ST) downstream and a mini diamond (MD) [27] upstream with a culet size of 200 µm without a bevel. To ensure quasi-hydrostatic conditions, argon was utilized as pressure transmitting medium. Rhenium of 200 µm thickness was used as gasket material. The pressure was determined by optical Raman spectroscopy of the diamond-anvil tip [28].

The (R)XES measurements were performed at beamline P01 of PETRA III (DESY) [29]. The X-rays were monochromatized by a Si(111) monochromator providing $\sim 6 \cdot 10^{13}$ ph/s at 10 keV incident energy with an energy resolution of 1.0 eV. An X-ray spot size of $7\,\mathrm{x}\,7\,\mu m^2$ was achieved at the sample position by focusing with a Kirkpatrick-Beatz mirror system. A wavelength-dispersive von Hámos spectrometer was applied in combination with a Pilatus 100K area detector to measure the emission spectra (schematic shown in Weis et al. [30]). It can be equipped with 4 cylindrically bent analyzer crystals of 500 mm bending radius dispersing the energy in the vertical direction and enabling focusing in the horizontal direction. The area detector allows for the detection of an emission spectrum in a single-shot fashion. We equipped the spectrometer with Si(111) and Si(110) analyzer crystals providing an energy resolution of ~ 0.5 eV and ~ 0.6 eV for iron Kα and Kβ emission detection, respectively, that is dominated by the pixel-size contribution of the detector ($172\,\mathrm{x}\,172\,\mu m^2$). The analyzer crystals are fixed to the spectrometer by magnetic backplates and can be exchanged quickly. The experimental geometries for iron Kα and Kβ emission using Si(333) and Si(440) analyzer crystal reflection are similar and the optimized vertical positions of the detector differ only by 2 cm. As the height of the detector's sensitive area is 8.38 cm, a simultaneous measurement of Kα and Kβ emission is possible. The spectrometer was set up at a horizontal scattering angle of $\sim 70°$ to optimize the field of view of the spectrometer regarding the sample contained in the DAC [31]. In this geometry, the signal-to-noise ratio is improved by a factor of 50 compared to emission detection in transmission geometry. Spectra of the single analyzers were energy calibrated, background corrected, and finally summed up. The acquisition time for iron vtc-XES was 60 minutes (30 min at 75 GPa) whereas measurements of the 1s2p RXES maps for 13 GPa and 75 GPa lasted 145 min and 50 min, respectively. Excellent data quality of the K$\beta_{1,3}$ emission can be obtained within minutes. All spectra are normalized to the area between 7020 eV and 7120 eV and are shown on an absolute energy scale except for spin-state analysis via Integral of Absolute Difference (IAD) method [32], where the K$\beta_{1,3}$ XES spectra are shifted in emission energy so that the center of gravity (COG) is at 7055 eV. IAD values are calculated between 7030 eV and 7070 eV. The first momentum (M_1) is calculated considering the intensity of the K$\beta_{1,3}$'s emission down to 50% of its maximum value according to Lafuerza et al. [33]. The shift of the M_1-position (ΔM_1) is scaled corresponding to a change in average spin of $\Delta S=2$ obtained via Fe_2O_3 spectra of a reference sample that was loaded together with FeO.

3. Results and Discussion

3.1. Iron $K\beta_{1,3}$ X-ray emission

Pressure-dependent iron $K\beta_{1,3}$ emission spectra of FeO are shown in Fig. 1. As LS reference for the IAD a spectrum of $FeCO_3$ measured at 82 GPa with the same setup is used (not shown here for clarity). The differences to the spectrum of FeO measured at 13 GPa (HS) were calculated and used for the determination of the IAD values and are presented in Fig. 1, shifted on y-scale for clarity. The inset shows the resulting IAD values in black and the ΔM_1 values in red. The grey dashed lines mark the limits of both IAD and ΔM_1 values for iron in pure HS and LS state. The IAD values start with an offset of 0.7 compared to the 13 GPa reference followed by a slow rise in IAD value with pressure in the rhombohedral phase. Up to 75 GPa, no HS to LS transition occurs. The observed offset is assigned to the structural transition at 16 GPa [7]. The symmetry of the crystal field is decreased in the rhombohedral phase, which splits the energy levels of the 3d electronic states further and influences the spectral shape of the $K\beta_{1,3}$ emission. For the higher pressures, the slow increase in IAD value is in accordance with that reported in the literature [26, 23, 24, 25] and may be assigned to the change in covalency during compression [33], potentially accompanied with the onset of the spin transition for the highest pressure.

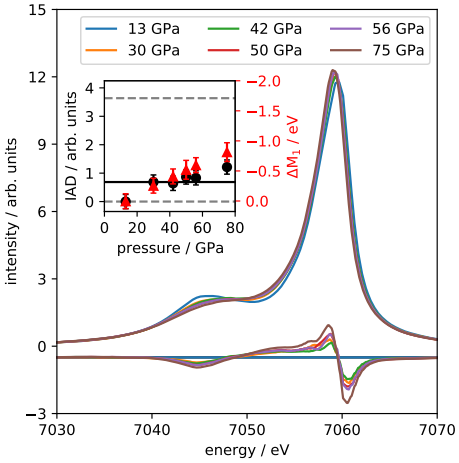

Figure 1. $K\beta_{1,3}$ spectra of FeO measured between 13 GPa and 75 GPa. The spectra are shifted to their COG for IAD analysis and the differences to the 13 GPa spectrum are set off vertically for clarity. The inset shows the IAD values in black and the ΔM_1 in red. The grey dashed lines correspond to the IAD and ΔM_1 values for pure HS and LS references.

3.2. Iron valence-to-core emission

Analysis of the vtc emission, visualized in Fig. 2, shows a good agreement with the previously mentioned literature. The vtc spectra have been extracted using a PearsonVII function to subtract the underlying tail of the $K\beta_{1,3}$ emission. The spectra are normalized to their corresponding $K\beta_{1,3}$ emission. The inset shows the integrated $K\beta$"-intensity. The $K\beta$" peak originates from the hybridization with oxygen's 2s orbitals and its intensity is connected to the Fe-O bonding distance [34]. The linear increase implies a nearly gradual decrease in bonding distance within the error of the experiment which we assign to the relatively small decrease of the FeO_6 octahedra with pressure, accompanied by the cubic to rhombohedral phase transition with a collapse in volume of only about 0.6% [5, 35]. Furthermore, the $K\beta$" peak position shifts constantly to lower energies which is connected to an increase in covalency with pressure

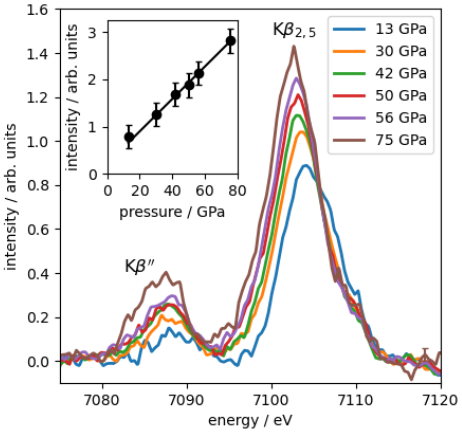

Figure 2. Iron vtc emission spectra of FeO measured between 13 GPa and 75 GPa. The inset shows the integrated intensity of the $K\beta''$ feature.

[22]. The K$\beta_{2,5}$ peak originates from the overlap between oxygen 2p and iron 3d states. Its peak shape shows a distinct variation between 13 GPa and 30 GPa with a significantly reduced contribution of the high-energy shoulder for higher pressure spectra.

3.3. Iron 1s2p RXES

At 13 GPa and 75 GPa 1s2p RXES maps were measured. The corresponding maps are visualized in Fig. 3 highlighting the pre-edge region in the grey boxes. Integration of a small area at constant emission energy (CEE) leads to X-ray absorption near edge structure spectra in the high-energy resolution fluorescence detected mode. The resulting CEE-cuts along with extracted pre-edge features are visualized in (b) for both pressures with a total integrated energy range of 1.75 eV in order to include all observable transitions. The data is scaled that both measurements overlap after the K-edge onset between 7130 eV and 7180 eV. The pre-edge features were extracted using an arctangent function. Following multiplet theory, a $3d^6$ transition metal in octahedral coordination and HS state has 3 electronic states in the pre-edge region, i.e., a lower energy $^4T_{1g}$ state, a $^4T_{2g}$ state, and a higher $^4T_{1g}$ state [36]. Due to the overlap of the multiplet states and the limited incident energy resolution, it is not possible to indicate those transitions unambiguously in the CEE-cuts for 13 GPa. At 75 GPa the whole pre-edge features are shifted to higher energies with the COG varying from 7112.92 ± 0.1 eV to 7113.26 ± 0.1 eV with a simultaneous FWHM (Full Width at Half Maximum) increase from ~ 3.3 eV to ~ 3.5 eV which is connected to an increased crystal field splitting by pressure. Furthermore, the rhombohedral unit cell causes a

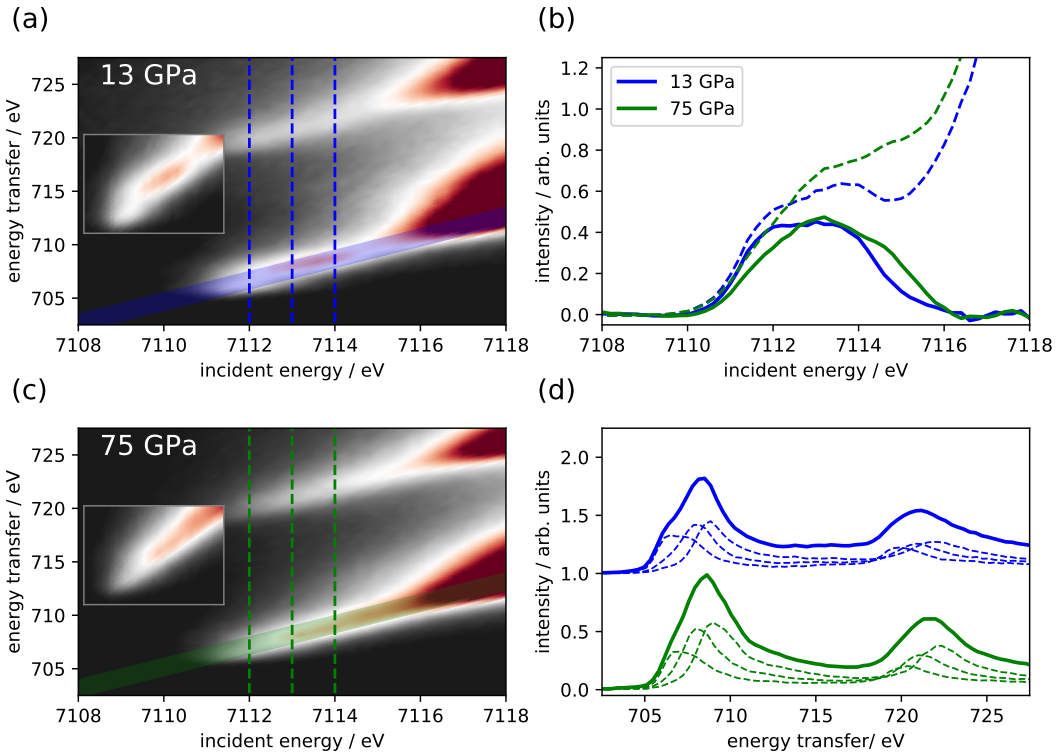

Figure 3. 1s2p RXES measurements of FeO at 13 GPa (a) and 75 GPa (c). (b) CEE-cuts with an integrated range of 1.75 eV for both pressures. The integrated ranges are highlighted by the shaded area in (a) and (c). (d) CIE-cuts at 7112 eV, 7113 eV, and 7114 eV (dashed) and the sum of these three cuts (solid).

change in crystal field splitting from a three-fold t_{2g} and a two-fold e_g into a non-degenerate a_{1g} and two two-fold e_g states [37] and thus smearing out of the transitions. Additionally, Yagi et al. [5] report a further distortion of the rhombohedral structure at pressures above 40 GPa which amplifies this effect.
Using the integration at constant incident energy (CIE) L-edge-like information can be obtained for 1s2p RXES. CIE-cuts were performed at incident energies of 7112 eV, 7113 eV, and 7114 eV and are visualized in Fig. 3 d). The solid lines represent the sum of the three cuts. In the comparison between both pressures, the COG of the L-edge is also shifted to higher energy transfer for the high-pressure spectra and the smearing out of the spectral shape is also reflected in the CIE-cuts. However, in the limits of the energy resolution, the general structure is conserved, which is in accordance with theory with no spin transition and iron still close to octahedral symmetry [5, 6, 7], different to the findings for $(Mg_{0.75}Fe_{0.25})O$ [19].

4. Conclusion

We presented a setup for (resonant) X-ray emission spectroscopy that enables a detailed analysis of the electronic structure of iron-bearing compounds at high pressure utilizing a dedicated scattering geometry in combination with data acquisition in a single-shot fashion via a von Hámos type spectrometer. The setup provides good data quality for vtc-XES under high-pressure conditions in less than one hour (30 min for 75 GPa). For RXES a Si(111) monochromator was used which provides an incident energy resolution of 1.0 eV. Based on the data quality after 50 min integration time, an acquisition time of around 3 hours can be estimated when using, e.g., a Si(311) monochromator in order to improve the incident energy resolution significantly to about 0.2 eV. The reached timescales for data acquisition suggest that high pressure can be coupled with temperature using laser heating [38] with this setup, for Kβ and vtc XES as well as RXES. As the energy resolution of emission detection is limited by the detector's pixel size, this can be significantly improved to about 0.2 eV when going from 172 µm to 50 µm pixels. Furthermore, the setup provides the opportunity to change the analyzer crystals to perform 1s3p RXES and the geometry allows also a combination of both crystal types simultaneously. Thus, it is a powerful tool for a complete analysis of the electronic structure of transition metals at high-pressure and high-temperature conditions.

Acknowledgments

We acknowledge DESY (Hamburg, Germany), a member of the Helmholtz Association HGF, for the provision of experimental facilities. This research was carried out at PETRA III beamline P01 in the scope of proposal I-20200600. We thank Conrad Hagemeister for technical support at P01, Christian Plückthun for providing the sample, and Lèlia Libon for gas loading at Deutsches GeoForschungsZentrum. This work was financially supported by the DFG via STE 1079/4-1 and WI 2000/17-1 within the DFG-FOR2125 CarboPaT and STE 1079/2-1.

References

[1] Irifune T, Shinmei T, McCammon C A, Miyajima N, Rubie D C and Frost D J 2010 *Science* **327** 193–195
[2] Sinmyo R and Hirose K 2013 *Phys. Chem. Minerals* **40** 107–113
[3] Prescher C, Langenhorst F, Dubrovinsky L S, Prakapenka V B and Miyajima N 2014 *Earth Planet. Sci. Lett.* **399** 86–91
[4] Piet H, Badro J, Nabiei F, Dennenwaldt T, Shim S H, Cantoni M, Hébert C and Gillet P 2016 *Proc. Natl. Acad. Sci. USA* **113** 11127–11130
[5] Yagi T, Suzuki T and Akimoto S I 1985 *J. Geophys. Res.* **90** 8784– 8788
[6] Fei Y and Mao H K 1994 *Science* **266** 1678–1680
[7] Mao H K, Shu J, Fei Y, Hu J and Hemley R J 1996 *Phys. Earth Planet. Inter.* **96** 135–145
[8] Fischer R A, Campbell A J, Shofner G A, Lord O T, Dera P and Prakapenka V B 2011 *Earth Planet. Sci. Lett.* **304** 496–502

[9] Speziale S, Milner A, Lee V E, Clark S M, Pasternak M P and Jeanloz R 2005 *Proc. Natl. Acad. Sci. USA* **102** 17918–17922
[10] Gavriliuk A G, Lin J F, Lyubutin I S and Struzhkin V V 2006 *JETP Lett.* **84** 161–166
[11] Kantor I Y, Dubrovinsky L S and Mccammon C A 2006 *Phys. Rev. B* **73** 100101
[12] Lin J F, Gavriliuk A G, Struzhkin V V, Jacobsen S D, Sturhahn W, Hu M Y, Chow P and Yoo C S 2006 *Phys. Rev. B* **73** 113107
[13] Lyubutin I S, Gavriliuk A G, Frolov K V, Lin J F and Troyan I A 2010 *JETP Lett.* **90** 617–622
[14] Solomatova N V, Jackson J M, Sturhahn W, Wicks J K, Zhao J, Toellner T S, Kalkan B and Steinhardt W M 2016 *Am. Mineral.* **101** 1084–1093
[15] Hamada M, Kamada S, Ohtani E, Sakamaki T, Mitsui T, Masuda R, Hirao N, Ohishi Y and Akasaka M 2021 *Phys. Rev. B* **103** 174108
[16] Badro J, Fiquet G, Guyot F, Rueff J P, Struzhkin V V, Vankó G and Monaco G 2003 *Science* **300** 789–791
[17] Lin J F, Struzhkin V V, Jacobsen S D, Hu M Y, Chow P, Kung J, Liu H, Mao H K and Hemley R J 2005 *Nature* **436** 377–380
[18] Lin J F, Vankó G, Jacobsen S D, Iota V, Struzhkin V V, Prakapenka V B, Kuznetsov A and Yoo C S 2007 *Science* **317** 1740–1743
[19] Lin J F, Mao Z, Jarrige I, Xiao Y, Chow P, Okuchi T, Hiraoka N and Jacobsen S D 2010 *Am. Mineral.* **95** 1125–1131
[20] Goncharov A F, Struzhkin V V and Jacobsen S D 2006 *Science* **312** 1205–1208
[21] Keppler H, Kantor I and Dubrovinsky L S 2007 *Am. Mineral.* **92** 433–436
[22] Schifferle L and Lobanov S S 2022 *ACS Earth and Space Chemistry* **6** 788–799
[23] Badro J, Struzhkin V V, Shu J, Hemley R J, Mao H K, Kao C C, Rueff J P and Shen G 1999 *Phys. Rev. Lett.* **83** 4101–4104
[24] Ozawa H, Hirose K, Ohta K, Ishii H, Hiraoka N, Ohishi Y and Seto Y 2011 *Phys. Rev. B* **84** 134417
[25] Hamada M, Kamada S, Ohtani E, Mitsui T, Masuda R, Sakamaki T, Suzuki N, Maeda F and Akasaka M 2016 *Phys. Rev. B* **93** 155165
[26] Pasternak M P, Taylor R D, Jeanloz R, Li X, Nguyen J H and Mccammon C A 1997 *Phys. Rev. Lett.* **79** 5046–5049
[27] Petitgirard S, Spiekermann G, Weis C, Sahle C, Sternemann C and Wilke M 2017 *J. Synchrotron Rad.* **24** 276–282
[28] Akahama Y and Kawamura H 2006 *J. Appl. Phys.* **100** 043516
[29] Wille H C, Franz H, Röhlsberger R, Caliebe A and Dill F U 2010 *J. Phys. Conf. Ser.* **217** 012008
[30] Weis C, Spiekermann G, Sternemann C, Harder M, Vankó G, Cerantola V, Sahle C J, Forov Y, Sakrowski R, Kupenko I, Petitgirard S, Yavaş H, Bressler C, Gawelda W, Tolan M and Wilke M 2019 *J. Anal. At. Spectrom.* **34** 384–393
[31] Albers C, Sakrowski R, Libon L, Spiekermann G, Winkler B, Schmidt C, Bayarjargal L, Cerantola V, Chariton S, Giordano N, Gretarsson H, Kaa J, Liermann H P, Sundermann M, Thiering N, Tolan Metin Wilke M and Sternemann C 2022 *Phys. Rev. B* **105** 085155
[32] Vankó G, Neisius T, Molnár G, Renz F, Kárpáti S, Shukla A and De Groot F M 2006 *J. Phys. Chem. B* **110** 11647–11653
[33] Lafuerza S, Carlantuono A, Retegan M and Glatzel P 2020 *Inorg. Chem.* **59** 12518–12535
[34] Spiekermann G, Harder M, Gilmore K, Zalden P, Sahle C J, Petitgirard S, Wilke M, Biedermann N, Weis C, Morgenroth W, Tse J S, Kulik E, Nishiyama N, Yavaş H and Sternemann C 2019 *Phys. Rev. X* **9** 011025
[35] Fei Y 1996 *Miner. Spectrosc.* **Special Publication 5** 243–254
[36] Westre T E, Kennepohl P, Dewitt J G, Hedman B, Hodgson K O, Solomon E I and V S U 1997 *J. Am. Chem. Soc.* **119** 6297–6314
[37] Karpishin T B, Stack T D P and Raymond K N 1993 *Am. Chem. Soc.* **115** 182–192
[38] Spiekermann G, Kupenko I, Petitgirard S, Harder M, Nyrow A, Weis C, Albers C, Biedermann N, Libon L, Sahle C J, Cerantola V, Glazyrin K, Konopkova Z, Sinmyo R, Morgenroth W, Sergueev I, Yavas H, Dubrovinsky L, Tolan M, Sternemann C and Wilke M 2020 *J. Synchrotron Radiat.* **27** 414–424